Nanoscale Advances

ROYAL SOCIETY OF CHEMISTRY

PAPER

View Article Online
View Journal | View Issue

Cite this: *Nanoscale Adv.*, 2025, **7**, 5193

Effect of the chemical nature of the nitrogen source on the physicochemical and optoelectronic properties of carbon quantum dots (CQDs)

Stephania Rosales,*[a] Karol Zapata,[a] Oscar E. Medina,[a] Benjamin A. Rojano,[b] Esteban A. Taborda,[a] Farid B. Cortés,[a] Agustín F. Pérez-Cadenas,[c] E. Bailón-García,[c] Francisco Carrasco-Marín[c] and Camilo A. Franco*[a]

This study investigates the influence of the chemical nature of nitrogen sources on the optical properties of Carbon Quantum Dots (CQDs) and evaluates their suitability for various industrial applications through a series of stability tests. Four nitrogen sources, —diethanolamine, diethylamine, ethylenediamine, and 1,2-phenylenediamine— were used to synthesize surface-active CQDs *via* a one-step microwave-assisted carbonization method. All CQDs exhibited a negative surface charge, ranging from −24.1 to −26.2 mV, indicating excellent colloidal stability at the working pH of 7. Nitrogen was successfully incorporated in all cases; however, CQDs synthesized with ethylenediamine and phenylenediamine showed significantly higher nitrogen contents. This increased incorporation was directly correlated with higher fluorescence quantum yields (QYs), reaching 20.44% with ethylenediamine and 22.61% with phenylenediamine, representing an improvement of up to 220% compared to those synthesized with other nitrogen sources. In addition to the nitrogen content, the carbon structure also influences the QY. Higher proportions of C=C bonds contribute to more extensive sp^2-conjugated domains, promoting electron delocalization and enhancing both electronic transitions and fluorescence efficiency. However, physical properties, such as particle size and thermal stability, remained unaffected by the choice of the nitrogen precursor. The CQDs demonstrated excellent thermal stability, ionic strength resistance, and long-term fluorescence retention, maintaining up to 90% of their initial fluorescence intensity under various storage conditions, making them suitable for use in harsh environments. However, an extremely acidic pH had the most detrimental effect, causing fluorescence intensity losses of up to 80% in CQD-phenylenediamine and CQD-diethylamine. These findings highlight the important role of nitrogen in enhancing the optoelectronic properties of the CQDs. Appropriate selection of the nitrogen source can significantly improve the fluorescence performance and optimize the response for practical applications.

Received 5th June 2025
Accepted 11th July 2025

DOI: 10.1039/d5na00554j

rsc.li/nanoscale-advances

Introduction

Carbon Quantum Dots (CQDs) are a type of nanomaterial in the carbon dot family, typically characterized by a nearly spherical morphology with both amorphous and crystalline cores. They are composed of graphitic or turbostratic carbon with sp^2 hybridization and often contain graphene or graphene oxide sheets fused or connected through sp^3-hybridized carbon atoms.[1] The synthesis of CQDs is generally categorized into top-down and bottom-up approaches, with the latter being more widely adopted owing to shorter reaction times and greater control over product properties.[2] Various precursors, including fruits, vegetables, organic waste[3] and human hair,[4] have been employed for CQD synthesis. However, despite the many synthesis routes proposed in the literature, achieving a high Quantum Yield (QY) remains a significant challenge. Since their discovery by Xu *et al.*,[5] extensive research has been conducted across multiple fields owing to their optical, electronic, and chemical properties such as high photoluminescence, biocompatibility, and ease of functionalization.[6] These attributes have made CQDs ideal candidates for applications in biomedicine, molecular sensing, optoelectronics, photocatalysis of contaminants, and the oil and gas industry.[7] Their optical behavior is primarily governed by the structure of the carbon core and nature of the chemical surface states.

[a]*Grupo de Investigación en Fenómenos de Superficie-Michael Polanyi, Departamento de Procesos y Energía, Facultad de Minas, Universidad Nacional de Colombia, Sede Medellín, Medellín 050034, Colombia. E-mail: srosalesd@unal.edu.co; caafrancoar@unal.edu.co*

[b]*Grupo de Investigación Química de los Productos Naturales y los Alimentos, Escuela de Química, Facultad de Ciencias, Universidad Nacional de Colombia, Sede Medellín, Medellín-Antioquia 050034, Colombia*

[c]*UGR-Carbon, Departamento de Química Inorgánica, Facultad de Ciencias—Unidad de Excelencia Química Aplicada a Biomedicina y Medioambiente, University of Granada, ES18071 Granada, Spain*

The doping of CQDs with heteroatoms, such as sulfur, nitrogen, oxygen, phosphorus, or boron, is a common strategy for enhancing quantum efficiency, optical properties, and dispersibility.[8] Among these, nitrogen is the most widely used, largely because it is inexpensive, simple, and readily accessible.[9] In addition, its small atomic size facilitates its incorporation into the CQD lattice. Its high electronegativity and the lone pair of electrons contribute to its chemical reactivity, enabling the formation of diverse bonding configurations. Nitrogen can form single, double, or triple bonds with carbon atoms, resulting in optically more active structures compared with undoped CQDs.[10]

Despite the widespread use of nitrogen in the production of CQDs, there is limited understanding of how the chemical nature of the nitrogen precursors affects the morphology, chemical characteristics, and optical behavior of the resulting materials. In many cases, the synthesis of nitrogen-doped CQDs (N-CQDs) relies on trial-and-error approaches. Although numerous methodologies have been reported in the literature, the specific role of the nitrogen source remains unclear. Commonly used precursors such as urea, melamine, glycine, and lysine[11] are often selected without a structured experimental design. However, N-CQDs frequently exhibit superior optical properties compared to those of regular CQDs. Their enhanced performance has enabled promising applications in biomedical imaging, biosensors drug delivery, photodynamic therapy, the detection of Reactive Oxygen Species, and antibacterial and antiviral agents.[12–14] In geosciences, N-CQDs have been used for environmental monitoring and contaminant detection, reservoir geology, rock and sediment studies, soil remediation, water quality monitoring and geothermal studies.[15–17] Although the choice of the nitrogen source is critical, it is often based on availability rather than on a rational or chemically guided selection process. Therefore, it is essential to systematically investigate the influence of different nitrogen precursors on the synthesis of CQDs.

To the best of our knowledge, this study provides the first systematic evaluation of different nitrogen sources, specifically primary and secondary amines with distinct structural features (aromatic and aliphatic). Additionally, robustness tests were performed to assess the stability of these nanomaterials. This approach aims to enhance our understanding of the structural, chemical, and optical implications of nitrogen doping in heavy-metal-free CQDs synthesized *via* simple and rapid methods. These findings contribute to the advancement of this emerging class of nanomaterials and support their potential scalability and broader adoption across various industries through demonstrated stability and performance at the laboratory scale.

Materials and methods

Materials

Anhydrous citric acid (United States Pharmacopeia-USP grade) was obtained from ProtoKimica (Medellín, Colombia). All other reagents were of analytical grade. Diethanolamine (Fig. 1a), NaOH, and HCl were purchased from Thermo Fisher Scientific (Waltham, MA). Diethylamine (Fig. 1b), ethylenediamine (Fig. 1c), and 1,2-phenylenediamine (Fig. 1d) were obtained from Sigma-Aldrich (St. Louis, MO, USA). All solutions for the experiments were prepared using distilled water.

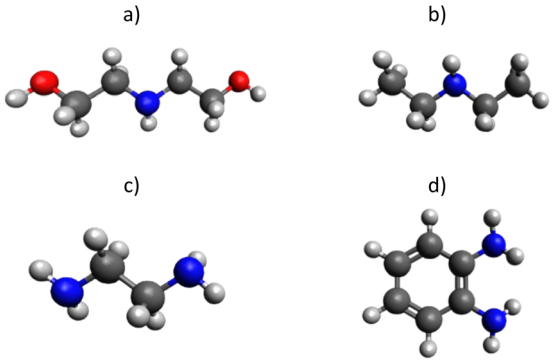

Fig. 1 Molecular models of the different sources of nitrogen used for the synthesis: (a) Diethanolamine, (b) diethylamine, (c) ethylenediamine, and (d) 1,2-phenylenediamine. Constructed with Avogadro 2.1 software.

Methods

CQDs synthesis. N-CQDs were synthesized using a modified microwave-assisted carbonization method based on a previously reported procedure.[18] Citric acid was used as the carbon source at 3.6 M, with a fixed mass ratio of 3 : 1 between citric acid and the nitrogen source. The nitrogen precursors used were diethanolamine, diethylamine, ethylenediamine, and 1,2-phenylenediamine, resulting in CQD-diethanolamine, CQD-diethylamine, CQD-ethylenediamine, and CQD-phenylenediamine, respectively. Distilled water was used as the synthetic solvent. Prior to carbonization, the mixtures were homogenized *via* ultrasonication to ensure the uniform dispersion of the precursors. Microwave-assisted carbonization was then performed at 600 W for 2 min in a GE 0.7 MGE07SEJ microwave (General Electric, USA). Following the synthesis, the products were cooled in a silica gel desiccator and subsequently redispersed in distilled water. The suspensions were filtered using 0.45 μm membrane filters, and the resulting CQDs were stored at 4 °C until further analysis.

To evaluate the effect of varying the amount of nitrogen precursor on the fluorescence quantum yield, an assay was conducted in which the mass ratio of citric acid to nitrogen precursor was modified. This evaluation focused on the CQDs that had previously shown the highest quantum yield when synthesized at a 3 : 1 ratio. The tested ratios included 3 : 0 (no nitrogen precursor), 3 : 0.5, 3 : 1.5, 3 : 2, and 3 : 3. All other synthesis steps were kept consistent with the previously described protocol. The quantum yield of each resulting sample was then measured.

CQDs characterization. Chemical characterization of the N-CQDs was performed by Fourier Transform Infrared Spectroscopy (FTIR), zeta potential analysis, and X-ray Photoelectron Spectroscopy (XPS). FTIR measurements were performed according to the protocol proposed by Siatis *et al.*,[19] using an IRAffinity-1 spectrometer (Shimadzu, Japan) in transmittance

mode, with a resolution of 2 cm^{-1} over the range of 4000–400 cm^{-1}. The zeta potential was determined *via* electrophoretic light scattering using a NanoPlus Zeta/nanoparticle analyzer (Micromeritics, Norcross, GA, USA) at room temperature.[20] XPS data were analyzed using XPS peak 4.1 software, applying a Shirley-type background correction and fitting the deconvoluted peaks with appropriate Gaussian–Lorentzian ratios.

Physical characterization was performed by measuring the hydrodynamic diameter, morphological analysis, and thermogravimetric analysis (TGA). The hydrodynamic diameter was determined by dynamic light scattering (DLS) using a NanoPlus Zeta/Nanoparticle Analyzer (Micromeritics, Norcross, GA, USA) under ambient conditions following the method described by Nassar *et al.*[21] Morphological analysis was conducted using Transmission Electron Microscopy (TEM) and images were captured using a Tecnai G2 F20 microscope (FEI, Hillsboro, OR, USA). Thermal stability was assessed following the protocol proposed by Medina *et al.*[22] using a high-pressure thermogravimetric analyzer (HP-TGA 750, TA Instruments Inc., Hüllhorst, Germany) with a heating ramp of 20 °C min^{-1} from 50 °C to 800 °C, at 0.084 MPa, and an airflow of 80 mL min^{-1}.

Optoelectronic properties, including light absorption and emission, were measured using UV-Vis absorption and fluorescence spectroscopy. UV-Vis spectra were recorded using a Shimadzu UV-1600i UV spectrometer (Kyoto, Japan) with 1 nm step intervals using standard quartz with a 10 mm optical path length. The fluorescence spectra were acquired using a Jasco FP-8350 spectrofluorometer. The QY was subsequently calculated using eqn (1):

$$\Phi = \Phi_{st} \times \left(\frac{K_c}{K_{st}}\right) \times \left(\frac{\eta_c}{\eta_{st}}\right)^2 \quad (1)$$

where Φ is the quantum yield, subscript "st" refers to the standard used for comparison, and "c" represents the CQD sample. Where K is the slope obtained from the integral fluorescence and absorbance curves. Where η is the refractive index of the solvent. Quinine sulfate (dissolved in 0.05 M H_2SO_4), with a known QY of 0.546, was used as the fluorescence standard.[23]

Stability tests for CQDs. A series of tests were designed to assess the stability of the N-CQDs under various conditions. Thermal stability was evaluated following the method proposed by Huang *et al.*[24] with slight modifications. The CQD dispersions were prepared at a concentration of 100 mg L^{-1} in distilled water and homogenized at 150 rpm for 15 min. The samples were then placed in ovens at controlled temperatures of 25 °C, 50 °C, and 70 °C for 2 h. The fluorescence emission intensity at the maximum wavelength was measured before and after the heating. The results are expressed as the % of the remaining fluorescence intensity relative to the unheated sample. The effect of ionic strength was evaluated using a modified protocol reported by Weidgans *et al.*[25] Sodium chloride (NaCl) solutions were prepared at concentrations of 500, 1000, 1000, 30 000, and 50 000 mg L^{-1} in distilled water. The CQDs were added to the saline solutions at 100 mg L^{-1}. The fluorescence emission intensity was measured for each sample and the results were reported as the remaining fluorescence intensity (%) compared to the intensity observed in pure water. Stability tests under storage time and pH conditions were conducted following a modified protocol proposed by Cristea *et al.*[26] For the storage test, CQD dispersions (100 mg L^{-1}) were stored in the dark at 25 °C for 2 months. Fluorescence emission intensity was measured at 0, 2, 10, 30, 45, and 60 d of storage. The results were reported as the remaining fluorescence intensity (%) compared to the initial fluorescence intensity. For the pH stability testing, solutions with pH levels between 2 and 14 were prepared using NaOH and HCl. Once the pH of the solution was adjusted, CQDs were dispersed at 100 mg L^{-1}. The fluorescence emission intensity was measured, and the results were reported as the remaining fluorescence intensity (%) compared to the maximum fluorescence intensity observed across the pH range. To assess the impact of these operating conditions on the optoelectronic properties of the CQDs, data analysis was performed using OriginPro 8.5 software. Statistical significance was evaluated using analysis of variance (ANOVA), followed by Tukey's post-hoc test, with a significance level set at $p < 0.05$.[27]

Results and discussion

Chemical characterization

FTIR analysis. FTIR spectra (Fig. 2) showed a band between 1703 and 1728 cm^{-1}, attributable to the stretching of the C=O bond present in carboxylic, esters and anhydrides configurations, as has been reported for carbon nanomaterials.[28] The signal observed between 1630 and 1632 cm^{-1} can be associated with the stretching of conjugated C=C bonds characteristic of the sp^2-carbons of CQDs.[29] as well as to the carbonyl group of amides, consistent with the incorporation of nitrogen into the carbon network of CQDs-N. The bands at 1368–1400 cm^{-1} correspond to deformations of methyl groups (CH_3) or to the symmetric stretching of COO^- carboxylates, while the regions of 1175–1217 and 1051–1061 cm^{-1} can be associated with the stretching of C–O (of ethers or alcohols) and C–N (of amines or amides) bonds of the CQD-N structures,[30] respectively. In addition, the presence of a broad band between 3298–3339 cm^{-1} suggests O–H and N–H stretching, characteristic of hydroxyl and/or amino groups.[31] confirming the hydrophilicity and N-functionalization of the CQDs structures. Together, these results indicate that the CQDs present a functionalized surface with polar oxygenated and nitrogenated groups, which confer water dispersibility and specific interactions, relevant in optoelectronic applications.

The identified functional groups are consistent with typical assignments of carbon quantum dots synthesized with citric acid and functionalized with oxygen and/or nitrogen.[32] This agreement indicates that the surface chemistry of the synthesized CQDs is comparable to that of similar nanomaterials described in previous studies.

Zeta potential. The functional groups on the surface of the CQDs provide a relatively negative surface charge. The zeta potential values for CQD-diethanolamine, CQD-diethylamine, CQD-ethylenediamine, and CQD-phenylenediamine at pH = 7.0 were −24.5 mV, −24.1 mV, −26.2 mV, and −24.1 mV

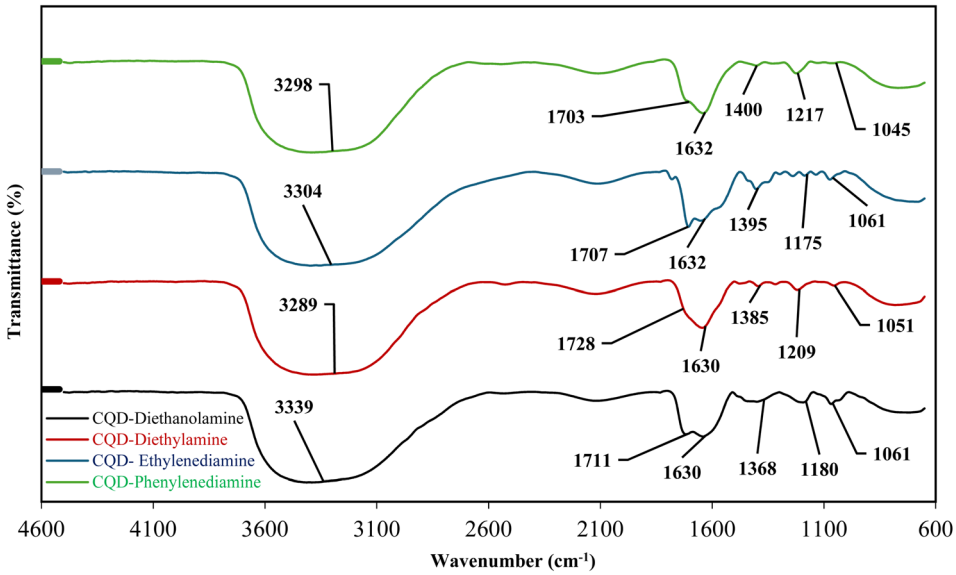

Fig. 2 The spectrum obtained by Fourier Transform Infrared Spectroscopy (FTIR) for the different CQDs synthesized by the microwave carbonization method.

respectively, indicating that the CQDs dispersions have high stability at working pH, resulting from the ionization of the carbonyl (C═O) and amine (–NH_2) groups present on the N-CQD surface.[33] Similar zeta potential values (−21.86 mV) have been reported for N-doped carbon quantum dots synthesized from castor seeds.[34] These studies indicate that the surface of such CQDs typically exhibits negative zeta potentials in the range of −15 to −30 mV, consistent with the presence of oxygen- and nitrogen-containing functional groups that contribute to colloidal stability and surface charge characteristics. Particularly zeta potentials far from zero under dispersion pH are desirable for commercial applications, as aggregation phenomena are not expected.

XPS analysis. The elemental composition of CQDs is not fixed, as it depends on the synthesis methods, precursors, and carbonization conditions used. Literature reports for similar nanomaterials indicate oxygen contents ranging from 15% to 55% and carbon contents between 20% and 70%.[35,35b,36] The surface composition of the synthesized CQDs falls within these ranges: XPS revealed carbon contents of 42.36–44.69%, oxygen contents of 38.92–48.16%, and nitrogen contents of 9.48–16.39% (Table 1). While carbon and oxygen contents remained relatively stable, nitrogen incorporation showed significant variation, depending on the nitrogen precursor. CQD-Ethylenediamine exhibited the highest nitrogen content (16.39%), attributed to the presence of two nitrogen atoms per molecule and its high reactivity during carbonization.

The high-resolution N_{1s} spectra (Fig. 3a) showed three main components centered at approximately 399.1 eV, 399.9 eV, and 400.6 eV, tentatively attributed to pyridinic-N, amine, and pyrrolic-N, respectively. These assignments are consistent with previous studies on nitrogen-doped carbon nanomaterials, though some overlap in peak positions is acknowledged.[37] Pyridinic-N, commonly found as N–C–N bonds, can be found in the core and surface of the CQD, while pyrrolic-N related to the N–H bond is exclusively found on the surface of the CQD.[37] Pyridinic and pyrrolic nitrogens are commonly associated with enhanced reactivity due to the availability of lone pair electrons, contributing to the chemical functionality of the CQDs.

The C_{1s} spectra displayed contributions from sp^2-hybridized carbon (C═C, ∼284.2 eV), ether (C–O–C, ∼287.2 eV), amine (C–N, ∼288.3 eV), and carboxylic acid (–COOH, ∼289.8 eV) groups. These assignments are broadly consistent with reported values for carbon-based quantum dots, although it is important to note that signal overlap may occur, particularly in the higher binding energy region.[37]

The O_{1s} spectra exhibited peaks at 529.9 eV (C═O) and 531.5 eV (C–O), suggesting the presence of carbonyl and hydroxyl functionalities on the CQD surface.

Notably, all N-CQDs synthesized exhibited a similar carbonaceous nature, with variations of ∼2%, characterized by relatively low sp^2 carbon content (C═C) and a predominant presence of carbon–oxygen–carbon linkages (C–O–C). Interestingly, the content of carboxylic acid groups (COOH) varied significantly among the samples. CQD-Diethanolamine and CQD-diethylamine exhibited the highest concentration of acidic functionalities (nearly 23.3%), whereas CQD-ethylenediamine had the lowest (around 1.3%). This is consistent with the basic nature of ethylenediamine, which contributes more N-groups while incorporating fewer oxygen-based groups.

Although the carbon content remained relatively constant across all samples, nitrogen incorporation varied by up to 7%, strongly influenced by the structure of the nitrogen precursor. For instance, ethylenediamine contains two nitrogen atoms and has a lower molecular weight, facilitating higher nitrogen incorporation (16.39%). In contrast, diethylamine, with one N-atom per molecule, resulted in a lower nitrogen content (9.48%) in the final CQD. Finally, an inverse relationship

Table 1 XPS analysis from C_{1s}, O_{1s} and N_{1s} spectra for N-CQDs[a]

Element	Material	Binding energy (eV)	Functional group	Contribution (%)	Total elemental%
C_{1s}	CQD-diethanolamine	284.2	C=C	14.94	43.75
		287.2	C–O–C	44.64	
		288.3	C–N	17.14	
		289.8	−COOH	23.26	
	CQD-diethylamine	284.2	C=C	15.29	42.35
		287.2	C–O–C	46.31	
		288.3	C–N	15.04	
		289.8	−COOH	23.34	
	CQD-ethylenediamine	284.2	C=C	19.65	44.69
		287.2	C–O–C	52.42	
		288.3	C–N	26.57	
		289.8	−COOH	1.34	
	CQD-phenylenediamine	284.2	C=C	19.20	43.30
		287.2	C–O–C	35.77	
		288.3	C–N/–OH	26.21	
		289.8	−COOH	18.80	
O_{1s}	CQD-diethanolamine	529.9	C=O	57.99	46.38
		531.5	C–O	42.01	
	CQD-diethylamine	529.9	C=O	55.81	48.16
		531.5	C–O	44.18	
	CQD-ethylenediamine	529.9	C=O	58.91	38.92
		531.5	C–O	41.08	
	CQD-phenylenediamine	529.9	C=O	54.16	42.06
		531.5	C–O	45.83	
N_{1s}	CQD-diethanolamine	399.1	Pyridinic-N	38.85	9.86
		399.9	Amine	50.44	
		400.6	Pyrrolic-N	10.69	
	CQD-diethylamine	399.1	Pyridinic-N	46.41	9.47
		399.9	Amine	44.51	
		400.6	Pyrrolic-N	9.07	
	CQD-ethylenediamine	399.1	Pyridinic-N	47.84	16.38
		399.9	Amine	46.43	
		400.6	Pyrrolic-N	5.72	
	CQD-phenylenediamine	399.1	Pyridinic-N	37.74	14.62
		399.9	Amine	45.39	
		400.6	Pyrrolic-N	16.86	

[a] The elemental percentages correspond to the atomic percentage (% atomic).

between nitrogen and oxygen content was observed, with more basic nitrogen precursors tending to reduce the presence of oxygen-containing acidic functional groups.[38]

All N-CQDs synthesized exhibited a similar carbonaceous nature, with variations of ~2%, characterized by relatively low sp^2 carbon content (C=C) and a predominant presence of carbon–oxygen–carbon linkages (C–O–C). Interestingly, the content of carboxylic acid groups (COOH) varied significantly among the samples. CQD-Diethanolamine and CQD-diethylamine exhibited the highest concentration of acidic functionalities (nearly 23.3%), whereas CQD-ethylenediamine had the lowest (around 1.3%). This is consistent with the basic nature of ethylenediamine, which contributes more N-groups while incorporating fewer oxygen-based groups.

Since, in all cases, a significant proportion of nitrogen was found on the CQD surface, it can be asserted that the synthesis strategy allowed the inclusion of this type of heteroatom in the CQD structure.[39] The structure of the precursors can be relevant during the functionalization of CQDs; in the case of CQD-ethylenediamine and CQD-phenylenediamine, the amino groups are located at the ends of the molecule, which can facilitate the modification of the number of holes and surface electrons in the CQD structure.[40]

The presence of pyrrolic and pyridinic nitrogen in the structure of CQDs suggests the formation of nitrogen-containing aromatic structures within the graphitic network of the material. Although none of the precursors used initially contain nitrogen in these forms, their detection in CQDs indicates that, during synthesis, the different nitrogen sources and citric acid self-assemble to create an extensive network.[41] This process occurs through the formation of amide bonds, resulting from intermolecular and intramolecular dehydration and polymerization among carboxyl, hydroxyl, and amine groups.[42] Consequently, a carbon core structure is obtained, in which nitrogen atoms are predominantly incorporated as pyridinic, pyrrolic, and amine entities, leading to the formation of N-CQDs.[37]

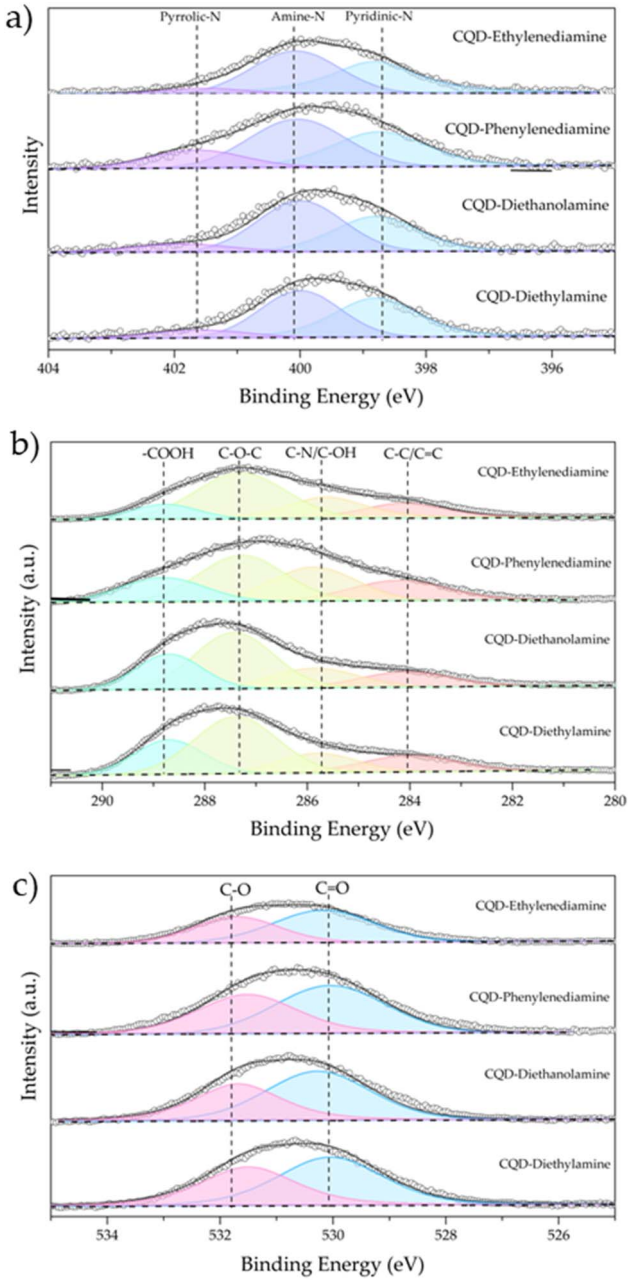

Fig. 3 High resolution (a) N_{1s}, (b) C_{1s} and (c) O_{1s} XPS spectra for CQD-diethanolamine, CQD-diethylamine, CQD-ethylenediamine and CQD-phenylenediamine.

To better understand the compositional correlation and chemical properties of the CQDs, correlations between the measured variables were performed. It was found that concerning the elements present on the surface of the CQDs and the zeta potential, the bonding configuration of oxygen to the carbon atom had an influence on the nanomaterial's charge potential. Specifically, a second-order polynomial correlation was observed in relation to the % of C═O. Lower C═O content corresponded to smaller zeta potential values, which also suggests that the presence of oxygen in the form of C–O promotes smaller negative potentials (Fig. 4).

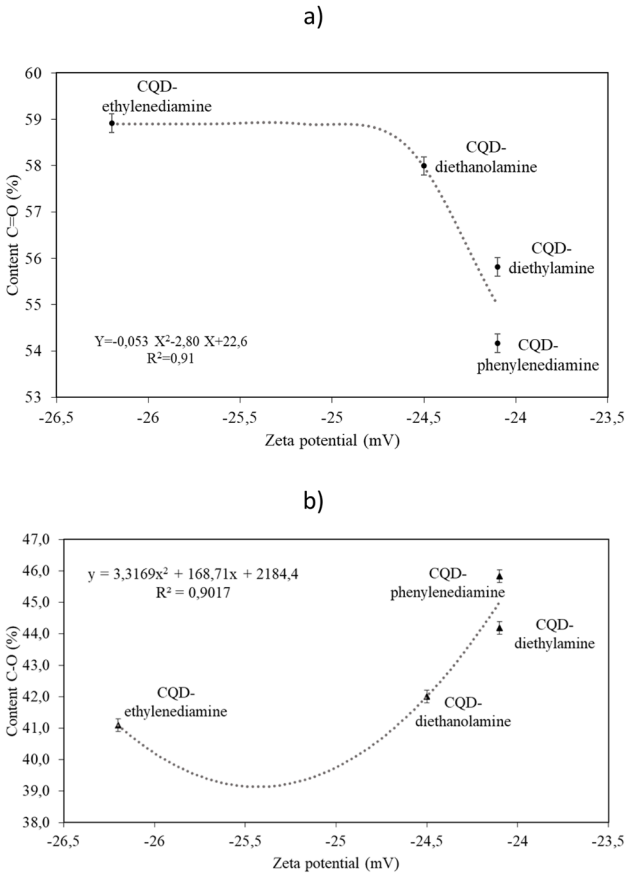

Fig. 4 Correlation between the z-potential and (a) the percentage of C═O content present on the surface of the synthesized CQDs and (b) the percentage of C–O content present on the surface of the synthesized CQDs.

The influence of how oxygen is bonded to carbon on the zeta potential may be related to the polarity of these functional groups. In particular, the carbonyl group (C═O) is more polar than the (C–O) group due to resonance effects.[43] Although the carbonyl group is not considered an acid, its presence can generate an inductive effect on neighboring groups, causing their polarization and consequently resulting in a surface with a greater negative charge.[44] On the other hand, C–O in the form of esters or non-deprotonated alcohols does not contribute to the generation of negative charge.

It is worth mentioning that the nitrogen incorporation pathways observed in the synthesized CQDs also offer valuable insights for the use of biomass-derived precursors. Many agro-industrial residues contain organic nitrogen primarily in the form of proteins, which are polymers of amino acids bearing primary amine groups. Under thermal treatment and carbonization conditions like those used in this study, these nitrogen-containing moieties can undergo dehydration and condensation reactions analogous to those proposed for the synthetic amines, leading to the incorporation of nitrogen into graphitic structures as pyridinic, pyrrolic, or amine species. Therefore, the results presented here support the feasibility of employing protein-rich biowastes as sustainable sources to produce N-doped CQDs, expanding the potential of circular and green synthesis routes.

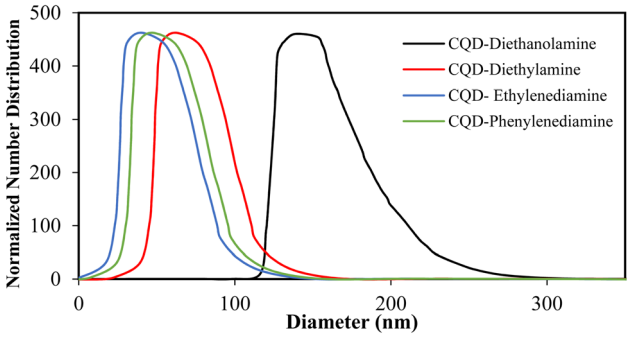

Fig. 5 Hydrodynamic diameter by DLS for synthesized N-CQDs.

Physical characterization

Hydrodynamic diameter. Fig. 5 shows the hydrodynamic diameter for synthesized N-CQDs. The recorded sizes were 138 ± 2 nm for CQD-diethanolamine, 61 ± 1 nm for CQD-diethylamine, 39 ± 2 nm for CQD-ethylenediamine and 46 ± 2 nm for CQD-phenylenediamine. The data reveals a clear decreasing size trend in the following order: CQD-diethanolamine > CQD-diethylamine > CQD-phenylenediamine > CQD-ethylenediamine.

Although the precursors used to obtain the CQDs undergo a transformation during the various stages of synthesis, their primary structure does influence the characteristics of the resulting CQDs. For example, it is possible that the hydroxyl groups at the ends of the diethanolamine used for the CQD-diethanolamine synthesis work as termination points during the polymerization reaction, remaining exposed at the edges of the CQD. A CQD with polar terminations reveals a greater number of hydrogen bonds with the surrounding water molecules, causing a considerable increase in hydrodynamic diameter.

TEM images. Fig. 6 shows the TEM results. The images allowed for the morphological observation of the N-CQDs, which were distinguished by their spherical or quasi-spherical shape. N-CQDs appear as dark-contrast regions against a lighter background due to their higher electron density compared to the support.[45] Diffraction patterns are often observed, indicating the presence of graphitic domains or graphene-like structures. In the obtained images are similar to the ones reported by Xu *et al.*[46] in witch this pattern is visible as consecutive parallel lines (highlighted sections in the images), confirming the successful synthesis of CQDs through a simple methodology and using various nitrogen sources.

The particle sizes determined by TEM were 11.55 nm for CQD-diethanolamine, 5.24 nm for CQD-diethylamine, 4.72 nm for CQD-phenylenediamine, and 4.04 nm for CQD-ethylenediamine.

The measured hydrodynamic diameters are consistently larger than the individual particle diameters determined by TEM. This disparity stems from the nature of each technique. TEM visualizes the solid, bare structure of the CQD, whereas DLS measures the effective size of the particle in solution. In an aqueous medium, CQDs are surrounded by a layer of solvent molecules, ions, and hydrated surface functional groups. This solvation layer moves cohesively with the nanoparticle,

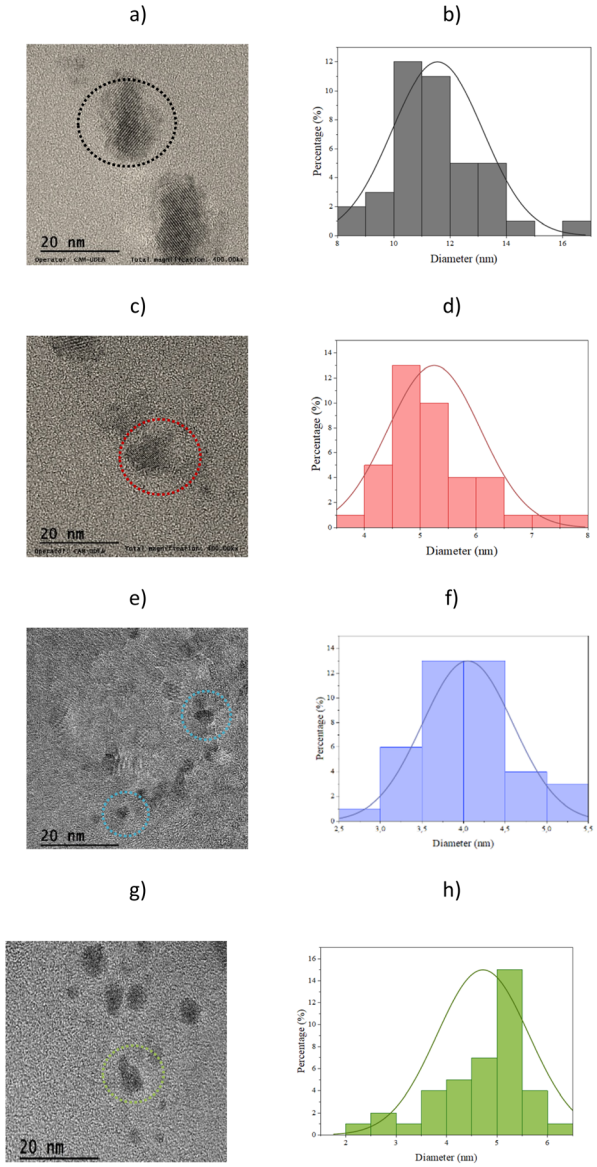

Fig. 6 High-resolution TEM images and diameter distribution for (a and b) CQD-diethanolamine, (c and d) CQD-diethylamine, (e and f) CQD-ethylenediamine, and (g and h) CQD-phenylenediamine.

increasing its apparent hydrodynamic volume and, consequently, the diameter measured in solution compared to the intrinsic size of the dry particle.[47] However, the size continued the decreasing trend observed in the DLS analysis, with CQD-diethanolamine > CQD-diethylamine > CQD-phenylenediamine > CQD-ethylenediamine, showing a positive association with the type of N precursor.

Thermogravimetric analysis. Fig. 7 presents the thermogravimetric analysis (TGA) curves of the synthesized N-CQDs. The results showed minimal mass loss (≤10%) at temperatures below 100 °C, which can be attributed to the evaporation of water molecules either present in the final dispersion or superficially adsorbed onto the surface of the CQDs.[48]

It is important to highlight that the degradation curves of CQD-diethanolamine and CQD-diethylamine show a single-

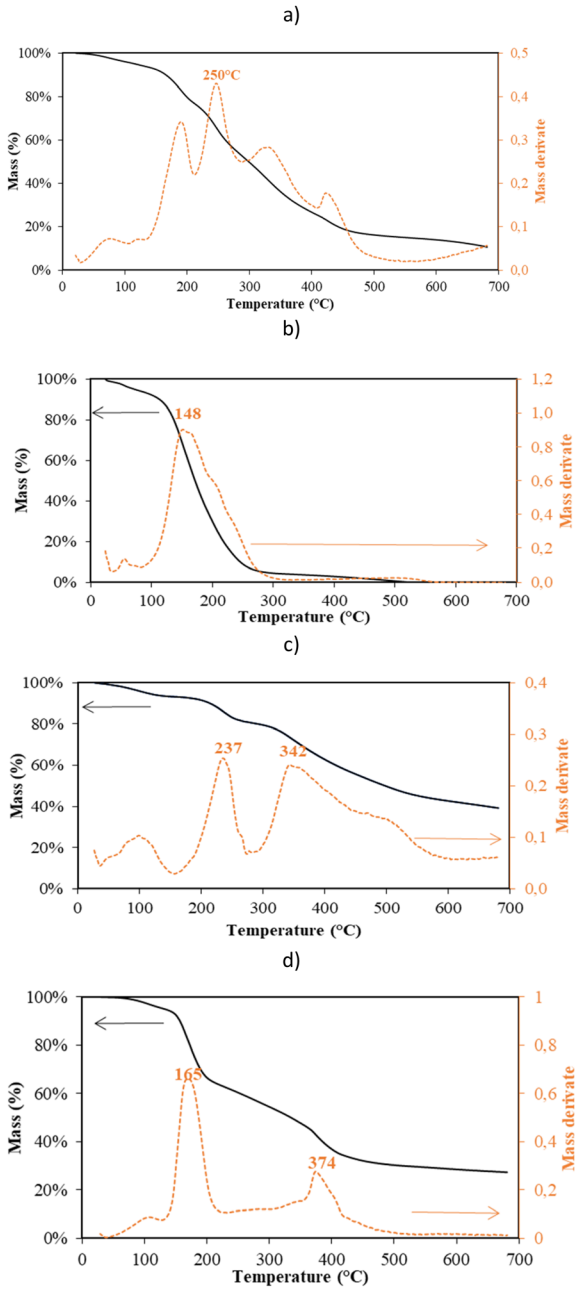

Fig. 7 Thermogravimetric curves for (a) CQD-diethanolamine, (b) CQD-diethylamine, (c) CQD-ethylenediamine, and (d) CQD-phenylenediamine, using a heating ramp of 20 °C min^{-1} from 50 °C to 800 °C under an air flow of 80 mL min^{-1}.

stage degradation profile, with no significant intermediate transitions. Maximum decomposition occurred at 250 °C and 148 °C. This behavior has been associated with simpler CQD structure, which may facilitate direct decomposition into low-molecular-weight volatile products. The XPS analysis showed that the percentage of C=C unsaturation in these two CQDs is lower than in CQDs with greater thermal stability. The abundance of carbon–carbon double bonds contributes to the formation of more rigid structures due to their higher bond energy (~614 kJ mol^{-1}) compared to C–C single bonds (~348 kJ mol^{-1}).[49] Therefore, a higher concentration of these bonds correlates with more rigid and compact structures, resembling graphitic or aromatic frameworks. This rigidity reduces atomic mobility and decreases the material's susceptibility to thermal degradation.

In contrast, CQD-ethylenediamine and CQD-phenylenediamine exhibited two-stage thermal degradation. The first degradation occurred above 200 °C and after the second beyond 300 °C. Notably, thermal degradation occurring above 400 °C is typically associated with highly graphitized domains in the CQD core.[50] Overall, these results indicate that CQD-ethylenediamine and CQD-phenylenediamine exhibit more complex structures and a highly stable carbon network.

This distinction is particularly relevant for practical applications. In many fields where CQDs are proposed as replacements for conventional tracers—such as in hydrogeological, agricultural, or construction studies—materials are generally subjected to ambient temperatures. In more demanding applications, such as those in the oil and gas industry, operational temperatures may vary depending on the reservoir and the recovery method.[51] Among the samples, CQD-ethylenediamine demonstrated the highest thermal stability above 400 °C, retaining approximately 40% of its initial mass. The behavior could be strongly related to the nitrogen source used during N-CQDs synthesis. The chemical nature of the nitrogen precursor is an essential factor for modulating the optical properties and generating thermally more resistant structures. Ethylenediamine, which contains two amino groups in its structure, can form strong covalent bonds with the core of the CQD, developing a more stable and reticulated network.[52] On the other hand, phenylenediamine, with its aromatic structure, offers an additional advantage in the formation of covalent bonds, as this precursor also allows the introduction of π–π interactions,[53] which favors graphitization and contributes to a more thermally resistant CQD structure. Conversely, diethanolamine contains hydroxyl groups that are more susceptible to thermal degradation and form weaker bonds with the carbon matrix. Diethylamine with fewer and less diverse functional groups, may lead to a simpler and less interconnected carbon framework, ultimately resulting in lower thermal stability.

Significant correlations between the evaluated physical properties and the surface composition of the CQDs were also investigated. The hydrodynamic diameter of the CQDs was found to have a significant correlation with the % carbon in the form of a double bond (C=C), as shown in Fig. 8.

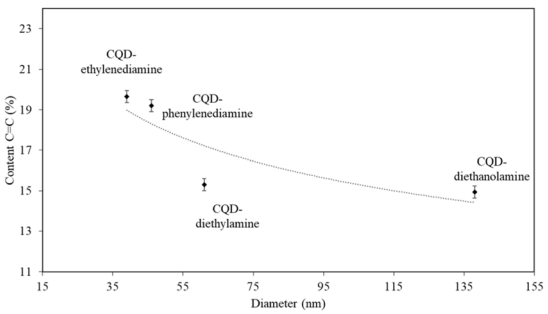

Fig. 8 Correlation between the content of C=C and the hydrodynamic diameter of the synthesized CQDs.

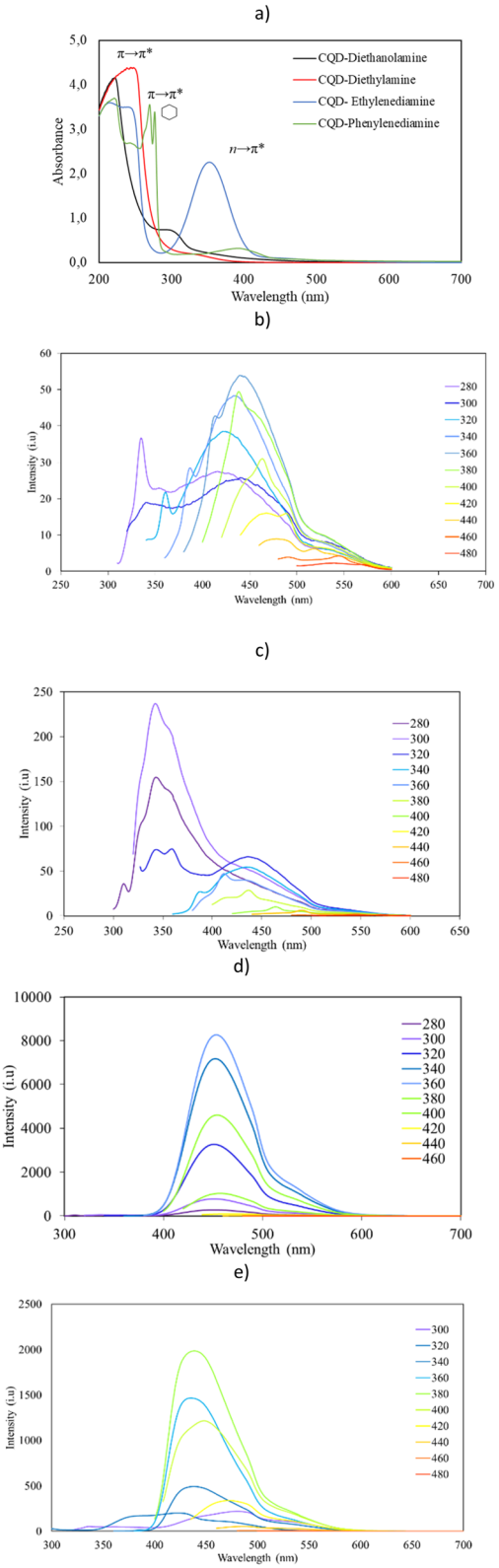

Fig. 9 (a) Absorbance spectra of CQD-diethanolamine, CQD-diethylamine, CQD-ethylenediamine, and CQD-phenylenediamine (b) fluorescence emission spectra at varying excitation wavelengths ranging from 280 nm to 480 nm for a CQD-diethanolamine water dispersion, (c) fluorescence emission spectra at varying excitation wavelengths ranging from 280 nm to 480 nm for a CQD-diethylamine water dispersion, (d) fluorescence emission spectra at varying excitation wavelengths ranging from 280 nm to 480 nm for a CQD-ethylenediamine water dispersion, and (e) fluorescence emission spectra at varying excitation wavelengths ranging from 280 nm to 480 nm for a CQD-phenylenediamine water dispersion.

While the reactions involved in the formation of the final CQD structure can vary depending on the synthesis precursors, the route, and the condition; one of the most studied stages is nucleation. This stage involves the formation of the initial carbon nuclei from which the structure will subsequently grow.[54] Finding a higher content of C=C bonds in CQDs with smaller sizes is attributed to a growth restriction process. The C=C bonds are more rigid and less prone to fusion,[55] which limits the structural reorganization of carbon atoms. Additionally, this type of bond favors the formation of aromatic rings and conjugated regions that are more stable but smaller compared to an extended graphitic structure dominated by single C–C bonds.

Optoelectronic characteristics. The UV-Vis absorption spectra for synthesized N-CQDs are shown in Fig. 9a. The results showed a typical pattern for CQDs with N groups.[56] A significant absorption peak was observed in the UV region (230–320 nm), along with an absorption tail extending into the visible region. With maximum absorption values of 221 nm, 250 nm, 215 nm, and 270 nm for CQD-diethanolamine, CQD-diethylamine, CQD-ethylenediamine, and CQD-phenylenediamine, respectively. This is in agreement with Vercelli *et al.*,[57] who synthesized CQDs from citric acid using urea as a nitrogen source.

The absorption spectrum of CQDs has been attributed to electronic transitions occurring within the material, which depend on its composition and structure. The peaks observed around 220–250 nm for all synthesized samples have commonly been associated with $\pi \rightarrow \pi^*$ transitions occurring in C=C bonds present in graphitic domains.[58] This result aligns with the diffraction pattern observed in the TEM micrographs. The absorption spectrum of CQD-phenylenediamine shows a second absorption region around 260–280 nm, which has been associated with $\pi \rightarrow \pi^*$ transitions in aromatic structures or more extended conjugated systems.[59] These systems contain multiple alternating double bonds or connected aromatic rings, allowing for greater π-electron delocalization throughout the CQD structure. In this sense, using a nitrogen precursor with an aromatic structure, such as phenylenediamine, could serve as a starting point in the synthesis to facilitate the formation of multi-ring connected structures. This is because phenylenediamine contains a stable aromatic ring, which can be incorporated into the carbon network during carbonization without undergoing complete breakdown.

The peaks observed between 320 and 400 nm have been associated with $n \rightarrow \pi^*$ transitions arising from heteroatom-containing functional groups, such as oxygen or nitrogen, present in C=O or C–N bonds.[60] Although all synthesized CQDs contain nitrogen in their structure, a higher proportion of this heteroatom was found in CQD-etilendiamine and CQD-phenylendiamine with N/C ratio up to 1.7 times higher compared to other N-CQD, which explained more pronounced bands in the region between 300–400 nm.

The fluorescence emission of CQDs varies depending on the excitation wavelength. CQD-Diethanolamine shows an excitation-dependent red shift when excited above 400 nm, while excitations at shorter wavelengths (≤360 nm) produce blue emissions, with a maximum at 445 nm. This behavior is attributed to nitrogen doping, and no fluorescence is detected beyond 480 nm. CQD-Diethylamine exhibits a distinct emission peak at 345 nm when excited between 280 and 300 nm, followed by a redshift for excitations between 320 and 400 nm. Emission is minimal above 440 nm. In contrast, CQD-ethylenediamine displays a fixed emission at 456 nm for excitation wavelengths ranging from 280 to 380 nm, with no fluorescence detected above 420 nm. CQD-phenylenediamine exhibits similar excitation-independent behavior, with a peak emission at 442 nm upon excitation at 380 nm. It also exhibits more degenerate spectra below 320 nm and no fluorescence beyond 400 nm. The maximum emission wavelengths observed were 445 nm (CQD-diethanolamine), 345 nm (CQD-diethylamine), 456 nm (CQD-ethylenediamine), and 442 nm (CQD-phenylenediamine). Most of these CQDs can be classified as violet/blue emitters, except CQD-diethylamine, which shows emission in the UV region as well as at 443 nm.

Despite using various nitrogen precursors for their synthesis, all CQDs exhibited a maximum fluorescence emission between 345–453 nm. This indicates that a significant redshift in emission is not primarily driven by the nitrogen source. Instead, it's more likely influenced by other experimental factors such as the carbonization method, reaction conditions (pressure, temperature, time), and the solvent used.[61] Therefore, modifying only the nitrogen precursor, without altering these other parameters, will not result in significant shifts in the emission wavelength.

The dependence of emission wavelength has been attributed to the introduction of energy levels between the nitrogen dopant and the $\pi \rightarrow \pi^*$ transitions of carbon in the CQD structure, resulting in multiple emission peaks.[62]

The main chemical difference affecting the CQD-diethylamine emission is the abundance of pyrrolic-N, as shown in the XPS analysis, the presence of pyrrolic nitrogen generates electronic defects within the carbon matrix, creating intermediate states within the band gap. These additional electronic levels can act as energy traps and modify the recombination dynamics of electrons.[63] The behavior observed in CQD-ethylenediamine and CQD-phenylenediamine differs from the commonly reported excitation-dependent emission in CQDs. The mechanisms explaining the fluorescent behavior in CQDs are related to oxygenated functional groups, quantum size effects, zigzag edge sites, defect effects, and electron–hole pair recombination.[64]

Mechanisms such as zigzag edge sites, quantum size effects, and electron–hole recombination are more plausible for single-emission centers, as observed in CQD-ethylenediamine and CQD-phenylenediamine. The coincidence of the excitation wavelength with the maximum peak in UV-Vis spectrum for CQD-ethylenediamine and CQD-phenylenediamine suggests that the fluorescence mechanism is associated with zigzag edge sites and $n \rightarrow \pi^*$ transitions of C=O groups. These findings imply that the latter two CQDs lack significant emissive traps or defect states, resulting in single-emission centers.

Table 2 QY values of the different N-CQDs

Sample	QY	N/C ratio	%N
CQD-diethanolamine	0.12	0.193	9.86
CQD-diethylamine	0.10	0.191	9.48
CQD-ethylenediamine	20.44	0.314	16.39
CQD-phenylenediamine	22.61	0.289	14.62

The QY results for synthesized CQDs are presented in Table 2. CQD-Ethylenediamine and CQD-phenylenediamine showed QY up to 200 times higher than other N-CQDs. Since the formation of CQDs involves oxidation, amination, and carbonization processes,[65] the variations in QY appear to be more closely linked to amination processes than to others. This conclusion is supported by the observation that CQDs with higher QY contain higher nitrogen content, and consequently, a higher N/C ratio on the surface of the CQD. Therefore, nitrogen sources that better facilitate the incorporation of nitrogen atoms into the carbon network of the CQD will enable the synthesis of nanomaterials with enhanced optical properties.

The reactivity and nature of the molecule containing the nitrogen atom appear to strongly influence the QY of the CQDs, as they condition their incorporation into the nanomaterial's structure and control the ease with which amination processes occur.

Due to the high-temperature conditions during the reaction and the nature of the precursors used in the synthesis (citric acid and primary or secondary amines), a plausible amination reaction for CQD formation is an amide condensation reaction.[66] This reaction occurs between the carboxylic acid groups (COOH) present in citric acid and an amine (primary, secondary, or even quaternary). The mechanism involves a nucleophilic attack by the nitrogen of the amine on the carbonyl carbon of citric acid, resulting in the formation of an amide bond (–CONH) and the elimination of a water molecule.[67] The mechanism of this reaction is illustrated in Fig. 10a.

Because the amide condensation reaction is considered one of the initial steps leading to the subsequent nucleation and growth of CQDs, its efficiency is crucial as it can significantly influence the following stages. Therefore, the selection of a nitrogen source for synthesis is critical. Among the precursors chosen in this study, primary amines (ethylenediamine and 1,2-phenylenediamine) yielded CQDs with noticeably higher quantum yields compared to those obtained using secondary amines (diethanolamine and diethylamine). The accessibility of the amino group on the exterior regions of the primary amine molecules facilitates their reaction with citric acid. In contrast, steric hindrance caused by carbon atoms surrounding the amino group of secondary amines might be limiting their efficiency as nitrogen sources for incorporation into the CQD structure, thereby affecting their optical properties (Fig. 10b).

In addition to steric and structural aspects, the electronic characteristics of each nitrogen source also play a key role in

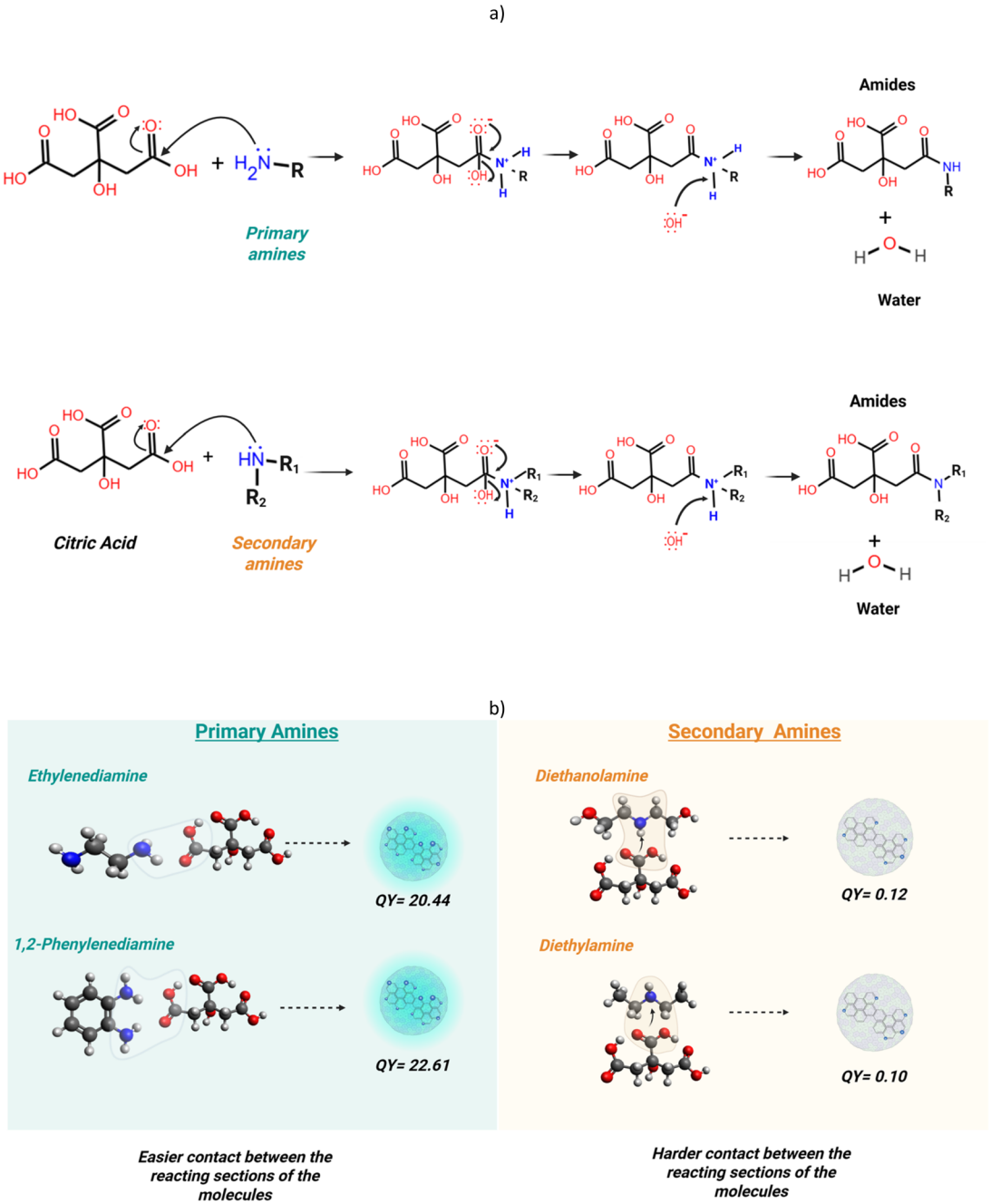

Fig. 10 (a) Reaction mechanism between citric acid and primary and secondary amines used for CQD synthesis, (b) schematic representation of the steric hindrance produced in the contact of citric acid with the primary and secondary amines used during the synthesis of CQDs.

determining QY. Nitrogen atoms can act as electron-donating sites within the CQD framework, facilitating radiative recombination by passivating surface traps and reducing non-radiative decay pathways. Primary amines tend to donate electrons more effectively and integrate more uniformly into the CQD matrix, promoting better surface passivation and enhancing photoluminescence. Conversely, secondary amines like diethanolamine and diethylamine may have lower electron-donating ability due to electron-withdrawing effects from adjacent alkyl or hydroxyl groups, leading to insufficient trap passivation and lower emission efficiency.[68] These effects highlight how both structural accessibility and electronic reactivity of nitrogen precursors converge to influence the optical performance of nitrogen-doped CQDs.

Also, hydroxyl groups of diethanolamine can form hydrogen bonds and interact with the environment, hindering contact with citric acid during the amination process. On the other hand, diethylamine presents a larger and less reactive structure than ethylenediamine and phenylenediamine, as the ethyl groups ($-CH_2CH_3$) are bulky and tend to interfere with the amination reaction.[69]

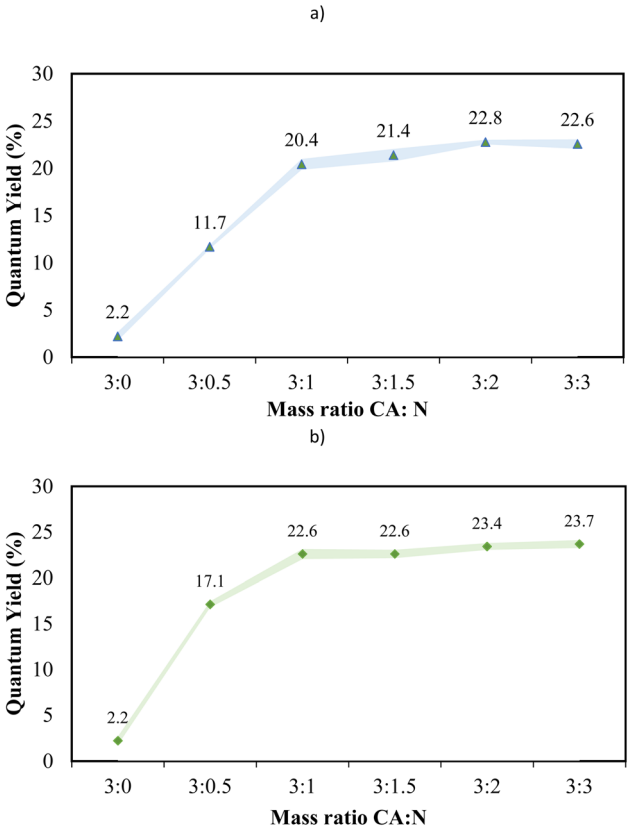

Fig. 11 The QY dependence on citric acid : N-precursor mass ratio used during the synthesis of (a) CQD-ethylenediamine and (b) CQD-phenylenediamine.

Given the significantly higher QY observed for CQD-ethylenediamine and CQD-phenylenediamine, an experiment was conducted to evaluate the effect of increasing the nitrogen precursor-to-citric acid ratio. The goal was to identify the optimal CA : N ratio for maximizing QY. The results are presented in Fig. 11.

The results showed that nitrogen sources can increase the QY of N-CQDs by up to 10 times compared to synthesis without an N-precursor. A control experiment using only ethylenediamine or phenylenediamine (without citric acid) yielded QYs of just 2.2% and 2.4% for CQD-ethylenediamine and CQD-phenylenediamine, respectively. This highlights the necessity of both citric acid and a nitrogen source for efficient CQD formation. While the nitrogen precursor plays a key role in enhancing QY, citric acid is essential during synthesis. It serves two main functions: (1) It provides reactive sites for interaction with ethylenediamine, phenylenediamine, and other citric acid molecules *via* its three carboxyl groups and one hydroxyl group,[57] and (2) it maintains a low pH in the reaction mixture, which acts as a catalyst for addition–elimination reactions,[70] such as Fischer esterification, that occur during the early stages of synthesis.

The relationship between nitrogen precursor content and the QY of CQD-ethylenediamine and CQD-phenylenediamine showed an asymptotic trend beyond a certain ratio. This plateau is likely due to the saturation of available binding sites on citric acid or stoichiometric limitations. A CA : N ratio of 3 : 1 yielded the highest QY for both systems. Beyond this ratio, further increases in nitrogen content resulted in minimal QY improvements—less than 2%—making additional nitrogen additions inefficient.

These findings highlight the importance of optimizing precursor ratios and reaction conditions to maximize QY while minimizing reagent consumption. It would be useful for future research to also evaluate the effect of the precursor's chemical nature on the QY parameter of CQDs.

Given their potential use as tracers, CQDs with higher QY enable fluorescence detection at lower concentrations, thereby reducing the required dosage and overall implementation costs. Proper selection and optimization of precursor quantities are, therefore, key for efficient and cost-effective applications.

Stability tests results. For the application of N-CQDs as tracers in various fields, it is essential to evaluate their stability

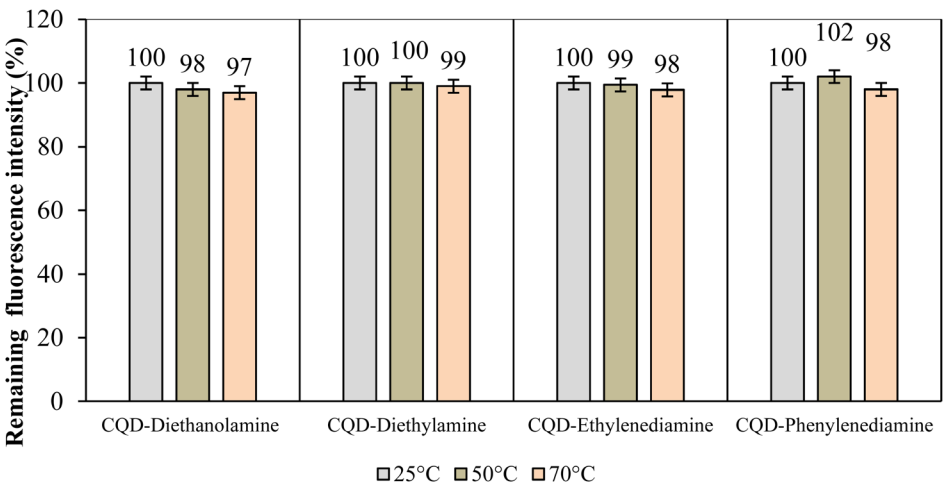

Fig. 12 Thermal stability evaluated through changes in the fluorescence for the N-CQDs prepared by dispersion in distilled water at 100 mg L^{-1} and subjected to 25, 50 and 70 °C.

under operational conditions. The influence of temperature, salinity, and storage time on the fluorescence emission of the synthesized N-CQDs is discussed below. Fig. 12 illustrates the effect of temperature on the emission properties of all N-CQDs. As shown, none of the samples exhibited significant fluorescence loss under the thermal conditions tested. This finding is consistent with the thermogravimetric analysis, which confirmed that the nanomaterials remain stable up to 100 °C.

The results showed that the observed variations in fluorescence intensity across the evaluated temperature range were statistically similar and fell within the expected experimental margin of error. This confirms that the CQDs maintain stable photoluminescent properties under thermal conditions, indicating that the emission is not significantly affected by temperature changes. These findings highlight the robustness and stability of the synthesized N-CQDs, making them suitable for applications where thermal fluctuations may occur.

The thermal resistance of CQDs can be attributed to structural and chemical factors. These nanomaterials are primarily composed of carbon atoms organized in either graphitic or amorphous structures. The covalent bonds within these structures provide high resistance to temperature increases.[71] Additionally, the high dispersibility of CQDs in water creates a stabilized medium where heat is uniformly dissipated, preventing the formation of hotspots that could promote thermal degradation.

Fig. 13 shows the effect of ionic strength on the fluorescence intensity of synthesized CQDs. The results revealed that in general, CQDs did not exhibited fluorescence attenuation under the evaluated saline conditions. Bayati *et al.*[72] have studied this phenomenon and suggest that CQDs functionalized with nitrogen show excellent stability in saline environments due to their surface chemistry, provided by amino groups. In this study, the dispersions of N-CQDs were prepared at high concentrations of NaCl, according to the salinity scale proposed by the United States Geological Survey (USGS), waters classified as highly saline can contain up to 35 000 mg L^{-1} of NaCl.[73] The results suggested that up to concentration of 30 000 mg L^{-1} the fluorescence intensity of the N-CQD suspension remained stable. However, even though animo groups offer optoelectronic stability to CQDs, other studies have established that the presence of pyrrole structures play an important role in mitigating cation-induced fluorescence quenching.[74] Due to the occurrence of a lone pair of electrons on the ring nitrogen in pyrrole groups that are capable of interacting with cations such as Na^+ through coordination or ion–dipole interactions to partially stabilize the cations in the surface environment of the material, preventing them from coming into direct contact with the emitting centers responsible for fluorescence, this explains why for CQD-ethylendiamine with lower pyrrole content by XPS – a quenching effect was evident at 50 000 ppm of ionic strength. Overall, the optical stability of CQDs at high salt concentrations reveals their potential for a wide range of industrial applications.

It's important to note that for CQD-diethanolamine, a slight increase in fluorescence was observed as a function of ionic strength; similar results were reported by Rhamanian *et al.*[75] When the salt concentration increases, the electrical double layer around the CQDs becomes compressed, leading to a reduction in electrostatic repulsion and thus promoting closer proximity between the dots. This interaction could be responsible for the increase in fluorescence intensity, as it enhances the energy transfer efficiency between the CQDs, improving the overall fluorescence emission.

Fig. 14 shows the results of evaluating the storage time (2 months) on the emission properties of the CQDs. As shown, the CQDs dispersion did not exhibit any variation in fluorescence intensity during the evaluation period. The fluorescence values measured at the end of the test were statistically identical to those recorded at the initial time (zero), demonstrating that CQDs are highly stable structures. This stability makes them suitable for applications requiring prolonged storage.

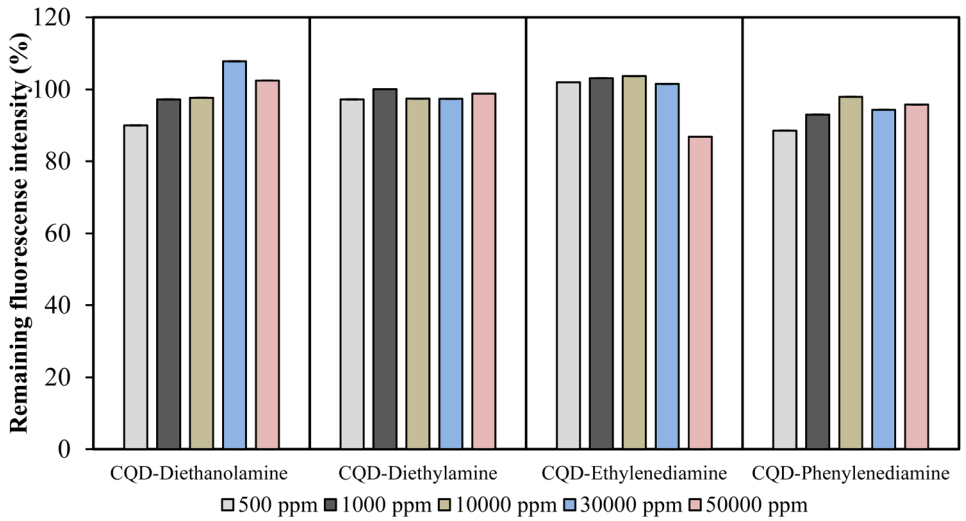

Fig. 13 Effect of ionic strength on the fluorescence of the N-CQDs prepared by dispersion in brine of the NaCl at 500, 1000, 10 000, 30 000, and 50 000 mg L^{-1}.

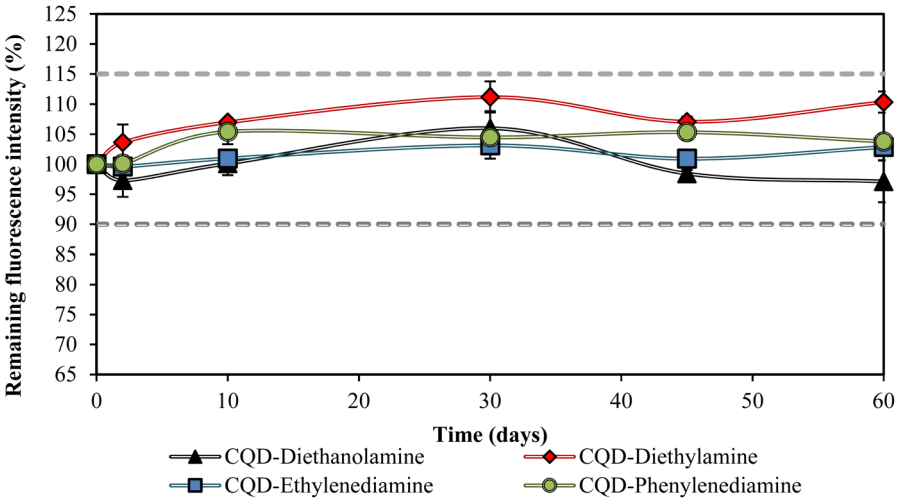

Fig. 14 Effect of storage time (2 months) on the fluorescence of N-CQDs prepared by dispersion in water at 100 mg L^{-1}.

The stability of these nanomaterials is attributed to both chemical and structural factors. The functional groups on the surface of CQDs play a critical role in maintaining optical stability, as they can stabilize the excited states and protect the emissive centers from fluorescence-quenching processes, such as collision-induced quenching.[76] Additionally, the core structure of the CQDs influences the emission efficiency and fluorescence stability. A well-organized core can minimize non-radiative energy losses, ensuring a stable fluorescence emission, as observed during the evaluation period.

As can be seen in Fig. 15 the pH significantly affects fluorescence intensity, with acidic pH values causing a reduction of up to 80% compared to the maximum intensity observed in the studied range.

The fluorescence intensity of CQD-diethylamine, CQD-ethylenediamine, and CQD-phenylenediamine was notably more affected by pH than that of CQD-diethanolamine. However, the best optical performance was observed at neutral or slightly alkaline pH levels. For CQD-diethylamine and CQD-phenylenediamine, a neutral pH resulted in significantly higher fluorescence intensity, whereas for CQD-ethylenediamine and CQD-diethanolamine, optimal optical performance was observed at a pH of 9. At acidic pH, the protonation of functional groups on the surface of the CQDs likely accounts for the reduction in fluorescence intensity.[77] In strongly acidic environments, protonation reduces the negative surface charge of the CQDs, promoting the formation of aggregates. Within these aggregates, non-radiative energy transfer occurs due to the overlap of CQDs, which diminishes fluorescence. This aggregation is minimized as the pH increases and approaches the optimal range. However, the opposite process occurs in a strongly alkaline environment. This repulsion hinders proximity between CQDs, reducing resonant energy transfer between particles and lowering

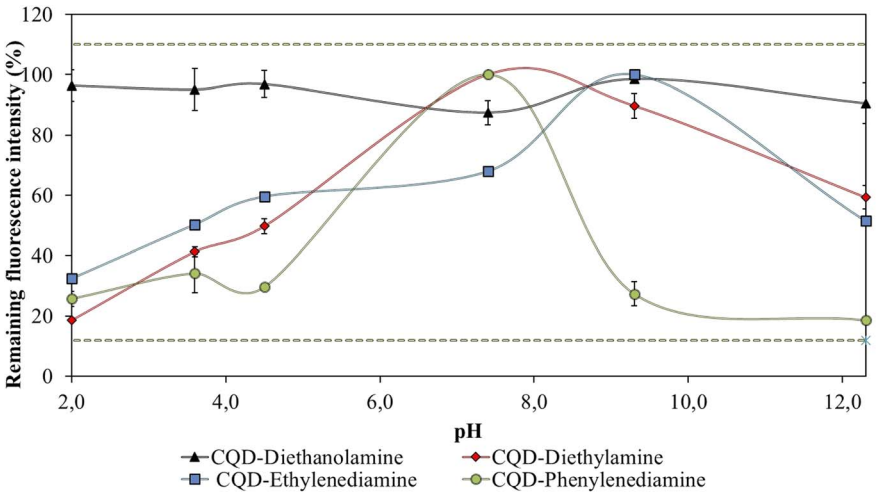

Fig. 15 Effect of pH e on the fluorescence of CQD-diethanolamine, CQD-diethylamine, CQD-ethylenediamine, and CQD-phenylenediamine prepared by dispersion in water at 100 mg L^{-1}.

fluorescence intensity.[78] In addition to surface-related processes, studies such as those by Zeng *et al.*[79] suggest that hydroxyl ions (OH^-) present in alkaline solutions can act as quenching agents. These ions may collide with the CQDs or chemically bind to their surface functional groups, promoting non-radiative deactivation of the excited states and thereby diminishing fluorescence emission. The ideal operational pH range for optimal fluorescence lies in neutral or slightly alkaline conditions. Therefore, the pH of the medium in which CQDs are used as tracers should be measured and, if possible, controlled to ensure better optical performance of the CQDs.

Conclusions

This study systematically investigated four different nitrogen sources with varying chemical natures, employed for the one-step, rapid synthesis of carbon *via* microwave-assisted carbonization. Characterization of the CQDs revealed that the nitrogen content directly influenced the fluorescence QY. Therefore, nitrogen precursors that promote the incorporation of heteroatoms into the CQD structure enable the synthesis of nanomaterials with enhanced optical properties. In this study, ethylenediamine and phenylenediamine were found to be superior. The structural characteristics of the precursor, including the positioning of the amino groups at the molecular terminals and cyclic geometry, appeared to facilitate nitrogen incorporation into the CQDs. Additionally, sp^2-hybridized carbon (C=C) is directly related to the fluorescence QY, likely due to the electronic transitions involved in fluorescence and the enhanced delocalization of charge carriers within these bonds. However, the physical properties of the CQDs, such as hydrodynamic size and particle size, did not appear to be significantly influenced by the nitrogen source used.

It is important to highlight that although higher nitrogen content leads to an increased QY, there is a precursor mass ratio beyond which no further improvement was observed. In this case, the QY does not significantly increase beyond a 3 : 1 carbon-to-nitrogen ratio, possibly because of the saturation effect. The CQDs exhibited different responses at varying excitation wavelengths; CQD-ethylenediamine and CQD-phenylenediamine displayed fixed emission behavior associated with their structure. No operating conditions, including temperature, salinity, or storage time, had a significant impact on the optical properties of the CQDs. However, a low pH attenuated the fluorescence emission of CQDs-N, likely due to the quenching effect caused by nanoparticle aggregation. These results highlight the emerging potential of this nanotechnology for the future replacement of conventional tracers, and the use of an appropriate nitrogen source enables the production of more efficient and stable CQDs.

Data availability

The authors declare that all the data in this manuscript are available upon request.

Author contributions

Stephania Rosales: Investigation, methodology, formal analysis, and writing – original draft. Karol Zapata: Methodology, writing – review & editing, Oscar E. Medina: Formal analysis, software, validation and writing – review & editing. Benjamin A. Rojano: Validation and writing – review & editing, Farid B. Cortés: Funding acquisition, supervision and writing – review & editing. Francisco Carrasco-Marín: Funding acquisition, methodology and writing – review & editing. E. Bailón-García: Supervision, formal analysis, methodology and writing – review & editing. Esteban A. Taborda: Validation and writing. Agustín F. Pérez-Cadenas: Supervision, formal analysis, methodology and writing – review & editing. Camilo A. Franco: Conceptualization, formal analysis, supervision and writing – review & editing.

Conflicts of interest

There are no conflicts to declare.

Acknowledgements

This research was funded by Fondo Francisco José de Caldas, MINCIENCIAS, and Agencia Nacional de Hidrocarburos (ANH) through Contract 112721-282-2023 (Project 1118-1035-9300) with Universidad Nacional de Colombia, Sede Medellín, and PAREX RESOURCES COLOMBIA AG SUCURSAL. And also supported by the Project PID2021-127803OB-I00 funded by MCIN/AEI/10.13039/501100011033/and by "ERDF A way of making Europe". The first author thanks the Universidad de Universidad Nacional de Colombia and the "Convocatoria para la formación de capital humano de alto nivel para el departamento de Nariño en el marco de la celebración del bicentenario y de la convocatoria 15 del plan bienal FCTel 2021–2022".

References

1 S. Gulati, A. Baul, A. Amar, R. Wadhwa, S. Kumar and R. S. Varma, Eco-friendly and sustainable pathways to photoluminescent carbon quantum dots (CQDs), *Nanomaterials*, 2023, **13**(3), 554.
2 W. Yang, X. Li, L. Fei, W. Liu, X. Liu, H. Xu and Y. Liu, A review on sustainable synthetic approaches toward photoluminescent quantum dots, *Green Chem.*, 2022, **24**(2), 675–700.
3 H. Fan, M. Zhang, B. Bhandari and C.-h. Yang, Food waste as a carbon source in carbon quantum dots technology and their applications in food safety detection, *Trends Food Sci. Technol.*, 2020, **95**, 86–96.
4 P. A. Kamble, R. P. Gambhir, A. A. Vibhute, V. S. Parkhe and A. P. Tiwari, A sustainable synthesis of functionalized carbon quantum dots from hair for the applications of cytotoxicity study and *in vitro* bioimaging, 2022, PREPRINT (Version 1) available at Research Square, DOI: **10.21203/rs.3.rs-2022101/v1**.
5 M. Saikia, T. Das, N. Dihingia, X. Fan, L. F. Silva and B. K. Saikia, Formation of carbon quantum dots and

graphene nanosheets from different abundant carbonaceous materials, *Diamond Relat. Mater.*, 2020, **106**, 107813.

6 (*a*) Y. Yao, H. Zhang, K. Hu, G. Nie, Y. Yang, Y. Wang, X. Duan and S. Wang, Carbon dots based photocatalysis for environmental applications, *J. Environ. Chem. Eng.*, 2022, **10**(2), 107336; (*b*) A. Xu, G. Wang, Y. Li, H. Dong, S. Yang, P. He and G. Ding, Carbon-based quantum dots with solid-state photoluminescent: mechanism, implementation, and application, *Small*, 2020, **16**(48), 2004621.

7 O. E. Medina, S. Rosales, N. Garzón, D. López, E. A. Taborda, J. C. Ordóñez, S. A. Fernández, F. B. Cortés and C. A. Franco, Advances in Quantum Dot Applications for the Oil and Gas Industry: Current Trends and Future Directions, *Energy Fuels*, 2024, **38**(22), 21793–21831.

8 (*a*) X. Kou, S. Jiang, S.-J. Park and L.-Y. Meng, A review: recent advances in preparations and applications of heteroatom-doped carbon quantum dots, *Dalton Trans.*, 2020, **49**(21), 6915–6938; (*b*) Z. Liu, W. Hou, H. Guo, Z. Wang, L. Wang and M. Wu, Functional group modulation in carbon quantum dots for accelerating photocatalytic CO2 reduction, *ACS Appl. Mater. Interfaces*, 2023, **15**(28), 33868–33877.

9 Ç. Kırbıyık, A. Toprak, C. Başlak, M. Kuş and M. Ersöz, Nitrogen-doped CQDs to enhance the power conversion efficiency of perovskite solar cells *via* surface passivation, *J. Alloys Compd.*, 2020, **832**, 154897.

10 L. T. Xu and T. H. Dunning Jr, Variations in the nature of triple bonds: The N2, HCN, and HC2H series, *J. Phys. Chem. A*, 2016, **120**(26), 4526–4533.

11 (*a*) J. Raut, R. D. Sherpa, S. K. Jana, S. M. Mandal, S. Mandal, S. P. Hui and P. Sahoo, N-Carbon Quantum Dot/Cu Complex for *In Vivo* Monitoring of Glycine Levels, *ACS Appl. Nano Mater.*, 2023, **6**(24), 23611–23619; (*b*) Y. Choi, N. Thongsai, A. Chae, S. Jo, E. B. Kang, P. Paoprasert, S. Y. Park and I. In, Microwave-assisted synthesis of luminescent and biocompatible lysine-based carbon quantum dots, *J. Ind. Eng. Chem.*, 2017, **47**, 329–335.

12 Q. Liu, C. Ma, X.-P. Liu, Y.-P. Wei, C.-J. Mao and J.-J. Zhu, A novel electrochemiluminescence biosensor for the detection of microRNAs based on a DNA functionalized nitrogen doped carbon quantum dots as signal enhancers, *Biosens. Bioelectron.*, 2017, **92**, 273–279.

13 (*a*) A. Karagianni, N. G. Tsierkezos, M. Prato, M. Terrones and K. V. Kordatos, Application of carbon-based quantum dots in photodynamic therapy, *Carbon*, 2023, **203**, 273–310; (*b*) O. Adegoke and P. B. Forbes, Challenges and advances in quantum dot fluorescent probes to detect reactive oxygen and nitrogen species: a review, *Anal. Chim. Acta*, 2015, **862**, 1–13; (*c*) S. S. Dwitya, Y.-H. Hsueh, S. S.-S. Wang and K.-S. Lin, Ultrafine nitrogen-doped graphene quantum dot structure and antibacterial activities against Bacillus subtilis 3610, *Mater. Chem. Phys.*, 2023, **295**, 127135; (*d*) N. A. Qandeel, A. A. El-Masry, M. Eid, M. A. Moustafa and R. El-Shaheny, Fast one-pot microwave-assisted green synthesis of highly fluorescent plant-inspired S, N-self-doped carbon quantum dots as a sensitive probe for the antiviral drug nitazoxanide and hemoglobin, *Anal. Chim. Acta*, 2023, **1237**, 340592.

14 N. Ziaee, N. Farhadian, K. Abnous, M. M. Matin, A. Khoshnood and E. Yaghoobi, Dual targeting of Mg/N doped-carbon quantum dots with folic and hyaluronic acid for targeted drug delivery and cell imaging, *Biomed. Pharmacother.*, 2023, **164**, 114971.

15 R. Gao, Z. Wu, L. Wang, J. Liu, Y. Deng, Z. Xiao, J. Fang and Y. Liang, Green preparation of fluorescent nitrogen-doped carbon quantum dots for sensitive detection of oxytetracycline in environmental samples, *Nanomaterials*, 2020, **10**(8), 1561.

16 W. S. Koe, W. C. Chong, Y. L. Pang, C. H. Koo, M. Ebrahim and A. W. Mohammad, Novel nitrogen and sulphur co-doped carbon quantum dots/titanium oxide photocatalytic membrane for in-situ degradation and removal of pharmaceutical compound, *J. Water Process Eng.*, 2020, **33**, 101068.

17 A. M. Ishmael, A. I. Abdel-Salam, M. M. Khalil and A. S. Mansour, Quantum Dots Composites for Energy Storage Applications, in *Quantum Dots Based Nanocomposites: Design, Fabrication and Emerging Applications*, Springer, 2024, pp. 429–454.

18 C. A. Franco, C. H. Candela, J. Gallego, J. Marin, L. E. Patiño, N. Ospina, E. Patiño, M. Molano, F. Villamil and K. M. Bernal, Easy and rapid synthesis of carbon quantum dots from Mortino (Vaccinium Meridionale Swartz) extract for use as green tracers in the oil and gas industry: Lab-to-field trial development in Colombia, *Ind. Eng. Chem. Res.*, 2020, **59**(25), 11359–11369.

19 N. Siatis, A. Kimbaris, C. Pappas, P. Tarantilis and M. Polissiou, Improvement of biodiesel production based on the application of ultrasound: monitoring of the procedure by FTIR spectroscopy, *J. Am. Oil Chem. Soc.*, 2006, **83**(1), 53–57.

20 S. Rosales, K. Zapata, F. B. Cortes, B. Rojano, C. Diaz, C. Cortes, D. Jaramillo, A. Vasquez, D. Ramirez and C. A. Franco, Simultaneous detection of carbon quantum dots as tracers for interwell connectivity evaluation in a pattern with two injection wells, *Nanomaterials*, 2024, **14**(9), 789.

21 N. N. Nassar, S. Betancur, S. C. Acevedo, C. A. Franco and F. B. Cortés, Development of a population balance model to describe the influence of shear and nanoparticles on the aggregation and fragmentation of asphaltene aggregates, *Ind. Eng. Chem. Res.*, 2015, **54**(33), 8201–8211.

22 O. E. Medina, I. Moncayo-Riascos, A. F. Pérez-Cadenas, F. Carrasco-Marín, C. A. Franco and F. B. Cortes, Experimental and theoretical study of the influence of solvent on asphaltene-aggregates thermo-oxidation through high-pressure thermogravimetric analysis, *Fuel*, 2023, **333**, 126491.

23 Y. Xie, J. Zheng, Y. Wang, J. Wang, Y. Yang, X. Liu and Y. Chen, One-step hydrothermal synthesis of fluorescence carbon quantum dots with high product yield and quantum yield, *Nanotechnology*, 2019, **30**(8), 085406.

24 J. Huang, Z. Hu, Y. Chin, Z. Pei, Q. Yao, J. Chen, D. Li and Y. Hu, Improved thermal stability of roselle anthocyanin by co-pigmented with oxalic acid: Preparation, characterization and enhancement mechanism, *Food Chem.*, 2023, **410**, 135407.

25 B. M. Weidgans, C. Krause, I. Klimant and O. S. Wolfbeis, Fluorescent pH sensors with negligible sensitivity to ionic strength, *Analyst*, 2004, **129**(7), 645–650.

26 E. Cristea, A. Ghendov-Mosanu, A. Patras, C. Socaciu, A. Pintea, C. Tudor and R. Sturza, The influence of temperature, storage conditions, pH, and ionic strength on the antioxidant activity and color parameters of rowan berry extracts, *Molecules*, 2021, **26**(13), 3786.

27 S. Karaj and J. Müller, Determination of physical, mechanical and chemical properties of seeds and kernels of Jatropha curcas L, *Ind. Crops Prod.*, 2010, **32**(2), 129–138.

28 K.-i. Takei, R. Takahashi and T. Noguchi, Correlation between the hydrogen-bond structures and the C=O stretching frequencies of carboxylic acids as studied by density functional theory calculations: Theoretical basis for interpretation of infrared bands of carboxylic groups in proteins, *J. Phys. Chem. B*, 2008, **112**(21), 6725–6731.

29 Z. Mirzaeifard and Z. Shariatinia, Economical, one-pot, and green synthesis of plant-based carbon quantum dots for efficient visible-light photocatalytic dye degradation and water purification, *J. Taiwan Inst. Chem. Eng.*, 2024, **163**, 105655.

30 U. Meraj, E. Laiq, R. Bushra, M. Ahmad, S. Gupta and M. Mujahid, Hydrothermal synthesis of okra waste-derived CQDs-CNTs nanocomposites: potent catalysts for pollutant degradation of RhB and MO dyes and its interaction with lysozyme protein, *Biomass Convers. Biorefin.*, 2025, 1–21.

31 Z. Li, Y. Du, Z. Zhang and D. Pang, Preparation and characterization of CdS quantum dots chitosan biocomposite, *React. Funct. Polym.*, 2003, **55**(1), 35–43.

32 S. Šafranko, K. Janđel, M. Kovačević, A. Stanković, M. Dutour Sikirić, Š. Mandić, A. Széchenyi, L. Glavaš Obrovac, M. Leventić and I. Strelec, A Facile synthetic approach toward obtaining N-Doped carbon quantum dots from citric acid and amino acids, and their application in selective detection of Fe (III) ions, *Chemosensors*, 2023, **11**(4), 205.

33 G. Midekessa, K. Godakumara, J. Ord, J. Viil, F. Lättekivi, K. Dissanayake, S. Kopanchuk, A. Rinken, A. Andronowska and S. Bhattacharjee, Zeta potential of extracellular vesicles: toward understanding the attributes that determine colloidal stability, *ACS Omega*, 2020, **5**(27), 16701–16710.

34 S. Elkun, M. Ghali, T. Sharshar and M. M. Mosaad, Green synthesis of fluorescent N-doped carbon quantum dots from castor seeds and their applications in cell imaging and pH sensing, *Sci. Rep.*, 2024, **14**(1), 27927.

35 (*a*) G. Gyulai, F. Ouanzi, I. Bertóti, M. Mohai, T. Kolonits and S. Bősze, Chemical structure and *in vitro* cellular uptake of luminescent carbon quantum dots prepared by solvothermal and microwave assisted techniques, *J. Colloid Interface Sci.*, 2019, **549**, 150–161; (*b*) B. Y. Yu and S.-Y. Kwak, Carbon quantum dots embedded with mesoporous hematite nanospheres as efficient visible light-active photocatalysts, *J. Mater. Chem.*, 2012, **22**(17), 8345–8353.

36 S. Y. Lim, W. Shen and Z. Gao, Carbon quantum dots and their applications, *Chem. Soc. Rev.*, 2015, **44**(1), 362–381.

37 S. D. Dsouza, M. Buerkle, P. Brunet, C. Maddi, D. B. Padmanaban, A. Morelli, A. F. Payam, P. Maguire, D. Mariotti and V. Svrcek, The importance of surface states in N-doped carbon quantum dots, *Carbon*, 2021, **183**, 1–11.

38 Y. Xu, J. Liu, C. Gao and E. Wang, Applications of carbon quantum dots in electrochemiluminescence: a mini review, *Electrochem. Commun.*, 2014, **48**, 151–154.

39 K. Bramhaiah, R. Bhuyan, S. Mandal, S. Kar, R. Prabhu, N. S. John, M. Gramlich, A. S. Urban and S. Bhattacharyya, Molecular, aromatic, and amorphous domains of N-carbon dots: leading toward the competitive photoluminescence and photocatalytic properties, *J. Phys. Chem. C*, 2021, **125**(7), 4299–4309.

40 S. Xue, P. Li, L. Sun, L. An, D. Qu, X. Wang and Z. Sun, The formation process and mechanism of carbon dots prepared from aromatic compounds as precursors: a review, *Small*, 2023, **19**(31), 2206180.

41 (*a*) M. J. Molaei, Principles, mechanisms, and application of carbon quantum dots in sensors: a review, *Anal. Methods*, 2020, **12**(10), 1266–1287; (*b*) L. Zhang, X. Yang, Z. Yin and L. Sun, A review on carbon quantum dots: Synthesis, photoluminescence mechanisms and applications, *Luminescence*, 2022, **37**(10), 1612–1638.

42 A. Antonelou, V. Benekou, V. Dracopoulos, M. Kollia and S. N. Yannopoulos, Laser-induced transformation of graphitic materials to two-dimensional graphene-like structures at ambient conditions, *Nanotechnology*, 2018, **29**(38), 384001.

43 S. Mitroka, S. Zimmeck, D. Troya and J. M. Tanko, How solvent modulates hydroxyl radical reactivity in hydrogen atom abstractions, *J. Am. Chem. Soc.*, 2010, **132**(9), 2907–2913.

44 H. Shabbir, E. Csapó and M. Wojnicki, Carbon quantum dots: the role of surface functional groups and proposed mechanisms for metal ion sensing, *Inorganics*, 2023, **11**(6), 262.

45 Y.-F. Kang, Y.-H. Li, Y.-W. Fang, Y. Xu, X.-M. Wei and X.-B. Yin, Carbon quantum dots for zebrafish fluorescence imaging, *Sci. Rep.*, 2015, **5**(1), 11835.

46 M. Xu, T. Liang, M. Shi and H. Chen, Graphene-like two-dimensional materials, *Chem. Rev.*, 2013, **113**(5), 3766–3798.

47 J. Lim, S. P. Yeap, H. X. Che and S. C. Low, Characterization of magnetic nanoparticle by dynamic light scattering, *Nanoscale Res. Lett.*, 2013, **8**, 1–14.

48 R. Ihly, J. Tolentino, Y. Liu, M. Gibbs and M. Law, The photothermal stability of PbS quantum dot solids, *ACS Nano*, 2011, **5**(10), 8175–8186.

49 S. Batsanov and L. Kozhevina, Energy of the C= C double bond, *Russ. J. Gen. Chem.*, 2004, **74**(2), 314–315.

50 S. R. Nxele and T. Nyokong, Time-dependent characterization of graphene quantum dots and graphitic

carbon nitride quantum dots synthesized by hydrothermal methods, *Diamond Relat. Mater.*, 2022, **121**, 108751.

51 M. A. Sohal, G. Thyne and E. G. Søgaard, Effect of the temperature on wettability and optimum wetting conditions for maximum oil recovery in a carbonate reservoir system, *Energy Fuels*, 2017, **31**(4), 3557–3566.

52 P. K. Yadav, S. Chandra, V. Kumar, D. Kumar and S. H. Hasan, Carbon quantum dots: synthesis, structure, properties, and catalytic applications for organic synthesis, *Catalysts*, 2023, **13**(2), 422.

53 J. Huang and M. Kertesz, Intermolecular covalent π− π bonding interaction indicated by bond distances, energy bands, and magnetism in biphenalenyl biradicaloid molecular crystal, *J. Am. Chem. Soc.*, 2007, **129**(6), 1634–1643.

54 J. Pan, A. a. O. El-Ballouli, L. Rollny, O. Voznyy, V. M. Burlakov, A. Goriely, E. H. Sargent and O. M. Bakr, Automated synthesis of photovoltaic-quality colloidal quantum dots using separate nucleation and growth stages, *ACS Nano*, 2013, **7**(11), 10158–10166.

55 Z. Liu, T. Lu and Q. Chen, Intermolecular interaction characteristics of the all-carboatomic ring, cyclo [18] carbon: Focusing on molecular adsorption and stacking, *Carbon*, 2021, **171**, 514–523.

56 (*a*) M. J. Molaei, The optical properties and solar energy conversion applications of carbon quantum dots: A review, *Sol. Energy*, 2020, **196**, 549–566; (*b*) G. E. LeCroy, F. Messina, A. Sciortino, C. E. Bunker, P. Wang, K. S. Fernando and Y.-P. Sun, Characteristic excitation wavelength dependence of fluorescence emissions in carbon "quantum" dots, *J. Phys. Chem. C*, 2017, **121**(50), 28180–28186.

57 B. Vercelli, R. Donnini, F. Ghezzi, A. Sansonetti, U. Giovanella and B. La Ferla, Nitrogen-doped carbon quantum dots obtained hydrothermally from citric acid and urea: The role of the specific nitrogen centers in their electrochemical and optical responses, *Electrochim. Acta*, 2021, **387**, 138557.

58 F. Yuan, Z. Wang, X. Li, Y. Li, Z. a. Tan, L. Fan and S. Yang, Bright multicolor bandgap fluorescent carbon quantum dots for electroluminescent light-emitting diodes, *Adv. Mater.*, 2017, **29**(3), 1604436.

59 G. Murali, J. K. R. Modigunta, S. Park, S. Lee, H. Lee, J. Yeon, H. Kim, Y. H. Park, S. Y. Park and J. R. Durrant, Enhancing light absorption and prolonging charge separation in carbon quantum dots *via* Cl-doping for visible-light-driven photocharge-transfer reactions, *ACS Appl. Mater. Interfaces*, 2021, **13**(29), 34648–34657.

60 D. Dai, X. Tu, X. Li, T. Lv and F. Han, Tuning solar absorption spectra *via* carbon quantum dots/VAE composite layer and efficiency enhancement for crystalline Si solar module, *Prog. Photovolt.: Res. Appl.*, 2019, **27**(4), 283–289.

61 X. Huo, H. Shen, R. Liu and J. Shao, Solvent effects on fluorescence properties of carbon dots: implications for multicolor imaging, *ACS Omega*, 2021, **6**(40), 26499–26508.

62 H. J. Yoo and B. E. Kwak, Competition of the roles of π-conjugated domain between emission center and quenching origin in the photoluminescence of carbon dots depending on the interparticle separation, *Carbon*, 2021, **183**, 560–570.

63 J. Li, A. Slassi, X. Han, D. Cornil, M. H. Ha-Thi, T. Pino, D. P. Debecker, C. Colbeau-Justin, J. Arbiol and J. Cornil, Tuning the electronic bandgap of graphdiyne by H-substitution to promote interfacial charge carrier separation for enhanced photocatalytic hydrogen production, *Adv. Funct. Mater.*, 2021, **31**(29), 2100994.

64 S. Mueller, J. Lüttig, L. Brenneis, D. Oron and T. Brixner, Observing multiexciton correlations in colloidal semiconductor quantum dots *via* multiple-quantum two-dimensional fluorescence spectroscopy, *ACS Nano*, 2021, **15**(3), 4647–4657.

65 M. Ali, A. S. Anjum, A. Bibi, S. Wageh, K. C. Sun and S. H. Jeong, Gradient heating-induced bi-phase synthesis of carbon quantum dots (CQDs) on graphene-coated carbon cloth for efficient photoelectrocatalysis, *Carbon*, 2022, **196**, 649–662.

66 R. M. Lanigan and T. D. Sheppard, Recent developments in amide synthesis: Direct amidation of carboxylic acids and transamidation reactions, *Eur. J. Org Chem.*, 2013, **2013**(33), 7453–7465.

67 H. Charville, D. A. Jackson, G. Hodges, A. Whiting and M. R. Wilson, *The Uncatalyzed Direct Amide Formation Reaction–Mechanism Studies and the Key Role of Carboxylic Acid H-Bonding*, Wiley Online Library, 2011.

68 F. Brotzel, Y. C. Chu and H. Mayr, Nucleophilicities of primary and secondary amines in water, *J. Org. Chem.*, 2007, **72**(10), 3679–3688.

69 M. Kienle, S. Reddy Dubbaka, K. Brade and P. Knochel, Modern amination reactions, *Eur. J. Org Chem.*, 2007, **2007**(25), 4166–4176.

70 H. Liu, Z. Zhang, J. Fang, M. Li, M. G. Sendeku, X. Wang, H. Wu, Y. Li, J. Ge and Z. Zhuang, Eliminating over-oxidation of ruthenium oxides by niobium for highly stable electrocatalytic oxygen evolution in acidic media, *Joule*, 2023, **7**(3), 558–573.

71 L. Hammer, N. J. Van Zee and R. Nicolaÿ, Dually crosslinked polymer networks incorporating dynamic covalent bonds, *Polymers*, 2021, **13**(3), 396.

72 M. Bayati, J. Dai, A. Zambrana, C. Rees and M. F. de Cortalezzi, Effect of water chemistry on the aggregation and photoluminescence behavior of carbon dots, *J. Environ. Sci.*, 2018, **65**, 223–235.

73 R. B. McCleskey, C. A. Cravotta III, M. P. Miller, F. Tillman, P. Stackelberg, K. J. Knierim and D. R. Wise, Salinity and total dissolved solids measurements for natural waters: An overview and a new salinity method based on specific conductance and water type, *Appl. Geochem.*, 2023, **154**, 105684.

74 J. Gaullier, M. Bazin, A. Valla, M. Giraud and R. Santus, Amino acid-pyrrole N-conjugates; a new class of antioxidants II. Effectiveness of singlet oxygen quenching by luminescence measurements, *J. Photochem. Photobiol., B*, 1995, **30**(2–3), 195–200.

75 O. Rahmanian, M. Dinari and M. K. Abdolmaleki, Carbon quantum dots/layered double hydroxide hybrid for fast and efficient decontamination of Cd (II): The adsorption kinetics and isotherms, *Appl. Surf. Sci.*, 2018, **428**, 272–279.
76 N. Javed and D. M. O'Carroll, Carbon dots and stability of their optical properties, *Part. Part. Syst. Charact.*, 2021, **38**(4), 2000271.
77 E. Rahmani, M. Pourmadadi, S. A. Ghorbanian, F. Yazdian, H. Rashedi and M. Navaee, Preparation of a pH-responsive chitosan-montmorillonite-nitrogen-doped carbon quantum dots nanocarrier for attenuating doxorubicin limitations in cancer therapy, *Eng. Life Sci.*, 2022, **22**(10), 634–649.
78 W. Liang, W. Zhang, X. Shao, K. Gong, C. Su, W. Zhang and C. Peng, Organic matters adsorbed on goethite inhibited the heterogeneous aggregation and adsorption of CdSe quantum dots: Experiments and extended DLVO theory, *J. Hazard. Mater.*, 2024, **467**, 133769.
79 B. Zeng, W. Xu, S. B. Khan, Y. Wang, J. Zhang, J. Yang, X. Su and Z. Lin, Preparation of sludge biochar rich in carboxyl/hydroxyl groups by quenching process and its excellent adsorption performance for Cr (VI), *Chemosphere*, 2021, **285**, 131439.